SEMARAK ILMU PUBLISHING

Semarak Journal of Thermal-Fluid Engineering

Journal homepage:
https://semarakilmu.my/index.php/sjotfe/index
ISSN: 3030-6639

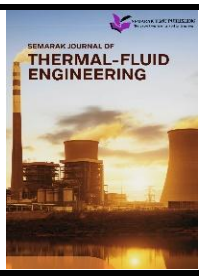


# Analysis of Flow Through a Sudden Expansion in a Pipe

Eng Shao Tang[1,*]

[1] Department of Mechanical Engineering, Faculty of Mechanical Engineering and Manufacturing, Universiti Tun Hussein Onn Malaysia, 86400 Batu Pahat, Johor, Malaysia

**ARTICLE INFO**

***Article history:***
Received 15 October 2025
Received in revised form 12 December 2025
Accepted 16 December 2025
Available online 21 December 2025

***Keywords:***
Computational fluid dynamics; sudden expansion; turbulence models; RANS; flow separation; k-epsilon; k-omega SST

**ABSTRACT**

Internal flow through a sudden pipe expansion is a fundamental problem in engineering and serves as a classic benchmark for Computational Fluid Dynamics (CFD). The abrupt change in geometry causes complex flow separation and the formation of a turbulent recirculation zone, which is notably difficult to model accurately. The purpose of this research is to investigate these complex flow dynamics and critically evaluate the performance of three common Reynolds-Averaged Navier-Stokes (RANS) turbulence models. A 3D model of a sudden expansion pipe was created and simulated using ANSYS. A steady-state, incompressible simulation was run with an inlet velocity of 1 m/s. A Grid Independence Test (GIT) was first conducted by comparing five different mesh densities, which validated an optimal grid for the main study. This grid was then used to compare the Standard k-ε, Realizable k-ε, and k-ω SST turbulence models. The principal results show a significant discrepancy between the models. Qualitatively, the Standard k-ε model predicted a much shorter potential core and earlier flow reattachment compared to the other formulations. Quantitatively, it emerged as a distinct outlier, predicting a much faster centerline velocity decay and a significantly deeper, more aggressive pressure drop just after the expansion. In contrast, the Realizable k-ε and k-ω SST models were in strong agreement with each other, both predicting a more gradual and similar flow recovery. The major conclusion is that the Standard k-ε model has low perceived accuracy for this application due to its known limitations in separated flows. The Realizable k-ε model and k-ω SST models are demonstrated to be far more reliable and accurate choices for this benchmark case.

## 1. Introduction

The study of internal fluid dynamics is a cornerstone of many engineering disciplines, fundamental to systems ranging from industrial pipelines to aerospace propulsion systems [1]. Understanding the behavior of internal flows, particularly under turbulent conditions, is essential for optimizing the performance, efficiency, and safety of these applications [2]. However, many practical engineering systems do not consist of simple, straight pipes but invariably include complex geometric features such as sudden expansions [3]. These components introduce significant complexities to the

* *Corresponding author.*
*E-mail address: dd220060@student.uthm.edu.my*

https://doi.org/10.37934/sjotfe.7.1.3851a

flow field, most notably flow separation, which creates recirculation zones and significantly increases pressure loss [4]. Accurately predicting these phenomena has traditionally relied on costly physical experiments, but Computational Fluid Dynamics (CFD) has emerged as an indispensable tool for solving governing equations over complex geometries [5]. The specific problem investigated in this study is turbulent flow through a sudden expansion, a geometry commonly used in heat exchangers and diffusers to manage flow velocity or promote mixing [6]. As fluid passes from the smaller inlet to the larger outlet, the abrupt area change causes the flow to detach from the wall, creating a high-velocity jet and a slow-moving recirculation zone [7].

The primary engineering challenge associated with this phenomenon is the significant energy loss from intense turbulence, which causes a substantial pressure drop [8]. Because of this defined challenge, the sudden expansion pipe is a classic benchmark case used extensively in the validation of CFD codes and, in particular, the performance of various turbulence models [9]. The primary aim of this study is to investigate these flow dynamics using ANSYS and to critically evaluate the performance of three Reynolds-Averaged Navier-Stokes (RANS) turbulence models: Standard k-ε, Realizable k-ε, and k-ω SST. To achieve this, the study first establishes an optimal mesh through a Grid Independence Test (GIT).

Subsequently, it analyzes and compares the pressure drops, centerline velocity profiles, and separation zone characteristics predicted by each model to determine their accuracy and reliability. Directly simulating all the chaotic, multi-scale eddies in a high-Reynolds-number turbulent flow, known as Direct Numerical Simulation (DNS), is computationally impossible for almost all practical engineering problems [10]. The computational power required scales prohibitively with the Reynolds number. To overcome this, the most common approach in industrial CFD is the Reynolds-Averaged Navier-Stokes (RANS) method. The core idea of RANS, developed by Osborne Reynolds, is to decompose instantaneous flow variables like velocity, $u$ into a time-averaged mean component, $\bar{u}$ and a fluctuating component, $u'$ as shown in Eq. (1).

$$u = \bar{u} + u' \tag{1}$$

When this decomposition is applied to the standard Navier-Stokes equations and then time-averaged, a new set of terms emerges. These terms, known as the Reynolds stresses, represent the effect of turbulent fluctuations on the mean flow. This process creates a fundamental dilemma: the averaging introduces more unknown variables than there are equations to solve. This is the famous "closure problem" of turbulence. A turbulence model is, therefore, a mathematical model required to close this system of equations. It provides a way to approximate the unknown Reynolds stresses in terms of the known mean flow quantities. The most popular method for this is the Boussinesq hypothesis, which assumes that the turbulent stresses behave similarly to viscous stresses, relating them to the mean velocity gradient via a new variable called the turbulent viscosity, $u_t$ [11].

The primary challenge then shifts to finding a way to calculate $u_t$. This is where models like k-ε and k-ω come in. They are known as "two-equation models" because they solve two additional transport equations, one for turbulent kinetic energy, k and another for its dissipation rate, ε or specific dissipation rate, ω. They are used to determine the turbulent viscosity, $u_t$ throughout the flow field. A critical decision in any RANS simulation is the choice of turbulence model, as it dictates how the Reynolds stresses are calculated. This, in turn, directly governs the accuracy of the simulation, especially in complex flows involving separation. This study compares three popular two-equation models. The Standard k-ε (k-epsilon) model, proposed by Launder and Spalding in 1974, is arguably the most widely used and validated turbulence model in industrial CFD [12]. Its enduring

popularity stems from its robustness, computational economy, and reasonable accuracy for a wide range of fully turbulent flows, particularly those that are not dominated by complex strains.

However, the Standard k-ε model has several well-documented limitations. It is derived assuming the flow is fully turbulent, which makes it reliant on "wall functions" to bridge the viscous sublayer near solid boundaries [13]. More critically for this study, the model is known to perform poorly for flows with adverse pressure gradients and strong flow separation. It often struggles to accurately predict the size of the recirculation zone and the reattachment length in problems like the sudden expansion. The Realizable k-ε model was developed to address the deficiencies of the standard model [12]. The term "realizable" means the model satisfies certain mathematical constraints on the Reynolds stresses, which are consistent with the physics of turbulence and which the standard model can violate.

This model features a new, improved formulation for the turbulent viscosity and a modified transport equation for the dissipation rate, ε. These changes lead to significantly better predictions for flows involving strong streamline curvature, vortices, and separation. It is generally more accurate than the standard k-ε model for predicting the behaviour of the recirculation zone in a sudden expansion, as it is more sensitive to the complex shear flows present in that region [14]. The Shear Stress Transport (SST) k-ω model, developed by Menter, is a highly regarded and robust hybrid model that combines the best features of both the k-ω and k-ε models [15]. It functions as a hybrid by intelligently blending two different formulations like it uses the standard k-ω model in the inner part of the boundary layer and the k-ε model in the free-stream.

Furthermore, this strategy is highly effective because it leverages the strengths of each model. The k-ω model is more accurate and robust for resolving the viscous sublayer directly at the wall, while the k-ε model is more reliable and avoids the k-ω model's problematic sensitivity to free-stream turbulence conditions [16]. Due to this intelligent blending, the k-ω SST model is widely considered to be superior for flows with adverse pressure gradients and significant flow separation. It is one of the most accurate RANS models for predicting reattachment points, making it a benchmark candidate for the sudden expansion problem.

## 2. Methodology

### *2.1 Geometry of Sudden Expansion of Pipe*

The geometry for this study was created using ANSYS Design Modeler with a "bottom-up" approach to extract the internal fluid domain from a solid pipe model. The process began by sketching and modeling the solid pipe walls as two separate cylinders which are an inlet cylinder with a length of 400 mm and an outer radius of 50 mm, and an outlet cylinder with a length of 400 mm and an outer radius of 100 mm. Once these solid bodies were created, the thin feature was applied with a uniform thickness of 5 mm. This operation hollowed out the solid cylinders, accurately representing the physical pipe structure.

Next, to create the computational domain, the fill tool was used. This feature automatically detected the enclosed internal volume of the hollow pipe and generated a new, separate body representing the fluid inside. This process resulted in two distinct bodies which are the pipe walls and internal flow domain. For the final CFD analysis, the pipe wall body was suppressed, ensuring that the solver would only mesh and compute the solution for the fluid domain. This final fluid domain is shown in Figure 1 below.

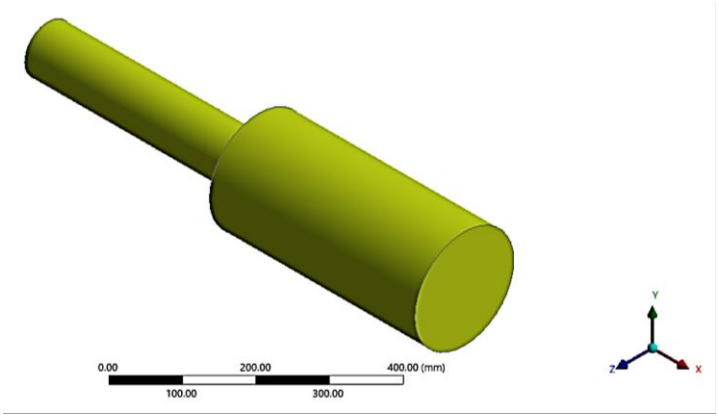


**Fig. 1.** Final 3D fluid domain extracted from the pipe geometry

### *2.2 Mesh Generation*

The process of meshing involves discretizing the entire 3D fluid domain into a finite number of small control volumes, or elements, over which the governing equations of fluid motion are numerically solved. This step is essential in CFD as it directly affects the accuracy, convergence, and computational cost of the simulation. In this study, meshing was performed using the ANSYS Meshing module. Before meshing, Named Selections were assigned to the critical boundaries, including "inlet", "outlet", and "wall". This ensures the correct identification and application of boundary conditions in the solver setup. A Hex Dominant Method was applied to the fluid body. This method prioritizes the creation of high-quality hexahedral elements, which can improve solution stability, while automatically incorporating other element types to conform to the complex geometry.

To systematically study the effect of the mesh on the solution, a series of five different meshes were created for the GIT. Mesh A, the coarsest, was generated using the default global Element Size of 42.196 mm with no additional refinement. Following this, meshes B, C, D, and E were created by applying a body sizing control to the entire fluid domain. This imposed a smaller, more refined element size, which was progressively reduced from 23 mm down to 19 mm to steadily increase the total element count. The refined mesh of the original model is illustrated in Figure 2, showing the detailed grid distribution throughout the domain.

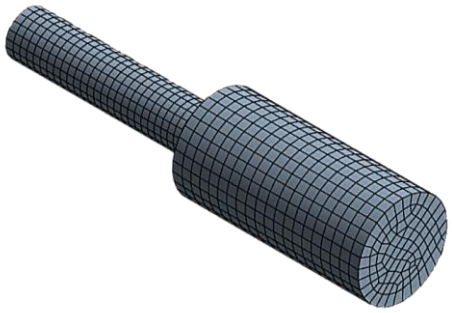

**Fig. 2.** Refined mesh original model

The goal was to find a balance between simulation accuracy and computational efficiency. While finer meshes offer better resolution of flow gradients, they require significantly more processing power. Conversely, coarse meshes reduce simulation time but can compromise result accuracy.

### *2.3 Grid Independence Test*

The GIT is an essential verification step in all CFD simulations. Its purpose is to ensure that the numerical results are independent of the mesh resolution and that further mesh refinement does not lead to significant changes in the output. This validation step is vital to confirm the accuracy and stability of the simulation outcomes, particularly for a flow problem involving separation. A balance must be achieved between computational cost and solution accuracy. Coarse meshes, like Mesh A, may produce results with large discretization errors, while overly fine meshes increase computational time and memory usage without delivering proportional improvements in accuracy [17]. Therefore, an optimal mesh resolution is determined by evaluating the deviation in a key result as the mesh is refined.

In this study, the GIT was conducted by evaluating the pressure drop across the sudden expansion pipe. It is calculated as the difference between the total pressure at the inlet and the total pressure at the outlet for five different mesh resolutions. The mesh was refined by progressively decreasing the Body Sizing, as detailed in the previous section. For each mesh, the pressure drop was calculated, and the percentage deviation between successive mesh configurations was computed using the formula, as shown in Eq. (2):

$$Deviation, \% = \frac{|\Delta P_{Mesh\ i+1} - \Delta P_{Mesh\ i}|}{\Delta P_{Mesh\ i+1}} \times 100 \quad (2)$$

where $\Delta P_i$ represents the pressure drop for the current mesh and $\Delta P_{i+1}$ represents the pressure drop for the next finer mesh.

### *2.4 Boundary Condition and Parameter Assumption*

In this simulation, boundary conditions were applied at the inlet, outlet, and wall boundaries to define the fluid behaviour throughout the pipe. These boundaries are illustrated in Figure 3. The inlet was assigned a velocity-inlet boundary condition with a uniform value of 1 m/s. At the outlet, a pressure-outlet condition of 0 Pa which is gauge pressure was imposed to allow the fluid to exit the domain freely and to establish a reference pressure for the simulation.

The walls of the sudden expansion pipe were treated with a no-slip boundary condition, which assumes zero relative velocity between the fluid and the solid surfaces. This setup is critical for accurately capturing near-wall effects such as boundary layer formation and the velocity gradients that lead to the flow separation at the expansion corner. For this study, the fluid was defined as water at standard conditions, with a density of 998.2 kg/m$^3$ and a dynamic viscosity, μ of 0.001003kg/m·s. The flow is treated as single-phase, incompressible, and turbulent.

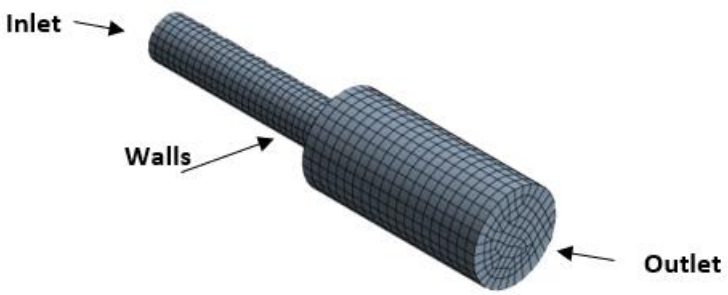


**Fig. 3.** Boundary zones

### *2.5 Governing Equation*

In CFD, the governing equations are essential mathematical expressions that describe the physical laws governing fluid behaviour. These equations form the foundation of the simulation process by encapsulating key conservation principles, specifically the conservation of mass and the conservation of momentum [18]. In this study, the flow is assumed to be steady-state, incompressible, and Newtonian. This means the fluid's density remains constant throughout the flow domain and that the shear stress is linearly proportional to the rate of deformation. Furthermore, the flow is considered isothermal, so the energy equation is excluded from the simulation scope.

#### *2.5.1 Continuity equation*

The Continuity Equation enforces the principle of mass conservation. It states that the rate of mass accumulation within a control volume must equal the net rate of mass flow into that volume [19]. This principle is essential for ensuring physically realistic results in CFD simulations. The general, unsteady form of the continuity equation is expressed as shown in Eq. (3):

$$\frac{\partial \rho}{\partial t} + \nabla \cdot (\rho u) = 0 \tag{3}$$

Here, ρ represents the fluid density, t is time, and u is the velocity vector. For this study, the flow is assumed to be steady-state, which means the flow properties do not change with time. Furthermore, the fluid is treated as incompressible, which means the density ρ is constant.

For a constant ρ, the density term can be factored out of the equation. The continuity equation thus simplifies considerably to its incompressible, steady-state form, which is used in this simulation as shown in Eq. (4):

$$\nabla \cdot u = 0 \tag{4}$$

This simplified form indicates that the divergence of the velocity field must be zero. In the context of this study, enforcing this equation is crucial for maintaining flow consistency and ensuring that no artificial sources or sinks of fluid are introduced, thereby preserving mass conservation across the entire sudden expansion domain.

#### *2.5.2 Momentum equation*

The Momentum Equation, commonly known as the Navier-Stokes equation, is derived from Newton's second law of motion. It describes the conservation of linear momentum in a fluid, governing how the velocity field evolves under the influence of various forces, such as pressure gradients and viscous stresses [20]. For the incompressible, Newtonian fluid in this study, these equations provide the foundational framework. However, since the flow is turbulent, the instantaneous equations are time-averaged to produce the RANS momentum equation. In this study, steady-state conditions are assumed and gravitational forces are considered negligible. The RANS momentum equation is therefore written as shown in Eq. (5):

$$\rho \left( \frac{\partial V}{\partial t} + V \cdot \nabla \mathrm{V} \right) = -\nabla \mathrm{p} + \mu \Delta^2 V + \rho g \tag{5}$$

where $\rho$ represents the fluid density, V is the velocity vector describing the direction and magnitude of the fluid flow, p denotes the static pressure within the fluid, $\mu$ is the dynamic viscosity which quantifies the fluid's resistance to shear or flow, and $g$ represents the gravitational acceleration acting on the fluid.

The RANS momentum equation, combined with the continuity equation, forms the foundation for this simulation. It enables the accurate analysis of velocity distribution, pressure gradients, and, most importantly, the flow recirculation and reattachment point after the sudden expansion. Solving this equation is essential for understanding the pressure loss and for comparing the performance of the different turbulence models.

### *2.6 Solver Execution*

The numerical solution of the governing equations in ANSYS Fluent was carried out using an iterative, pressure-based solver. This approach involves updating the solution variables over multiple cycles until the results stabilize and no longer change. This process is closely monitored by tracking residuals, which measure the error or imbalance in each conservation equation at every iteration. In this simulation, the standard residual convergence criteria were set to $1 \times 10^{-4}$. This means that each equation is considered to be satisfactorily solved once its normalized residual falls below this threshold.

The solution's convergence behaviour is illustrated in Figure 4. The simulation was run for approximately 210 iterations, by which point all residuals had stabilized. The residuals for x-velocity, y-velocity, and z-velocity show excellent convergence, all dropping below $1 \times 10^{-5}$. The turbulence residuals, k and epsilon, also successfully met the $1 \times 10^{-4}$ target.

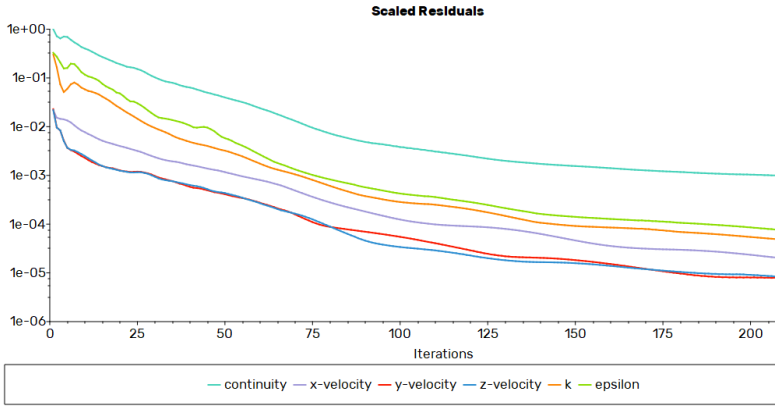


**Fig. 4.** Residual plot for the converged solution

The continuity residual, while being the highest, stabilized and flattened out at a value of approximately $1 \times 10^{-3}$. In CFD, a converged solution is indicated not just by residuals passing a specific threshold, but also by their stabilization. The consistent downward trend and subsequent flattening of all residual plots is a strong indicator of a stable and successfully converged solution, ensuring that the fluid flow variables were no longer changing significantly between iterations.

### *2.7 Post-Processing Setup*

After obtaining a converged solution in ANSYS Fluent, the results file was loaded into the CFD-Post module for analysis. This step involved creating the specific plots and visualizations required for the analysis in Chapter 4. To visualize the overall flow field, velocity contours and static pressure contours were generated. Since the model is 3D, these contours were plotted on a 2D mid-plane that slices through the center of the pipe. To analyze the flow separation, streamlines were generated starting from the inlet. Streamlines depict the path followed by fluid particles, helping identify areas of smooth flow, recirculation, or stagnation. This method is used to visualize the path of the fluid and clearly identify the boundaries of the recirculation zone. Finally, to create the quantitative graphs for comparison, data was extracted along specific geometry lines, including a line along the pipe centerline for the velocity and pressure plot.

## 3. Results and Discussion

### *3.1 Verification Results of Sudden Expansion of the Pipe*

Before comparing the different turbulence models, the Grid Independence Test (GIT) results were analyzed to select an optimal mesh. This ensures that the subsequent physics analysis is not influenced by discretization errors. The pressure drop across the pipe was calculated for five progressively finer meshes, as summarized in Table 1. Figure 5 provides a visual comparison of the static pressure along the pipe's centerline for all five meshes. It clearly shows that Mesh A is a significant outlier, predicting a much lower pressure drop. As the mesh is refined from Mesh B to Mesh E, the pressure profile curves begin to converge, especially in the critical recirculation and recovery zones.

**Table 1**
Grid independence test results

| Mesh | Element size (mm) | Body sizing (mm) | Number of elements | Number of nodes | Pressure Inlet (Pa) | Pressure outlet (Pa) | Pressure drop (Pa) | Deviation (%) |
|---|---|---|---|---|---|---|---|---|
| A | 42.196 | - | 3850 | 3438 | -79.80 | 0.00 | 79.80 | 19.53 |
| B | 42.196 | 23 | 5232 | 4508 | -99.17 | 0.00 | 99.17 | 9.52 |
| C | 42.196 | 21 | 5260 | 4982 | -90.55 | 0.00 | 90.55 | 2.73 |
| D | 42.196 | 20 | 5795 | 5185 | -93.10 | 0.00 | 93.10 | 1.93 |
| E | 42.196 | 19 | 6568 | 5724 | -94.93 | 0.00 | 94.93 | - |

The convergence behaviour is further quantified in Figure 6, which plots the calculated Pressure Drop versus the Number of Nodes. The solution does not follow a smooth, monotonic trend initially; the pressure drop fluctuates between Mesh A, B, and C, likely due to the coarse nature of this initial meshes being unable to consistently capture the complex recirculation zone. However, as the mesh is further refined, the pressure drop stabilizes.

The deviation between mesh C and mesh D is 2.73%, and the deviation betweenm D and the finest mesh, mesh E, drops to 1.93%. Since this change is small and the solution is clearly stabilizing, mesh D was selected as the optimal mesh. It contains 5795 elements and 5185 nodes, effectively balancing simulation accuracy and computational demand. Consequently, mesh D provides reliable, mesh-independent results and was used for all subsequent turbulence model comparisons.

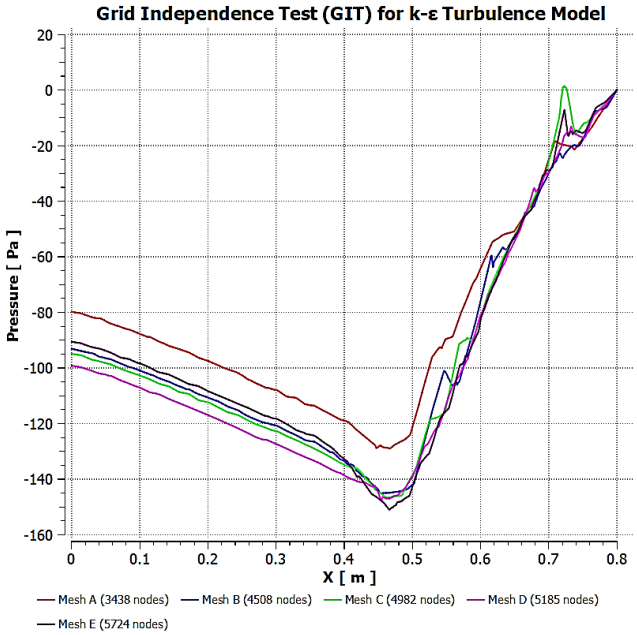


**Fig. 5.** Static pressure along the centerline for all five meshes

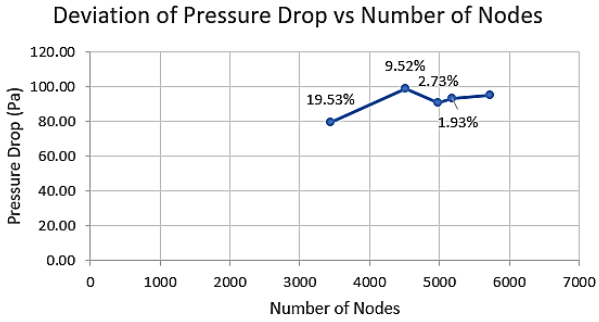


**Fig. 6.** Deviation of pressure drop versus number of nodes

### *3.2 Qualitative Flow Analysis of Sudden Expansion in a Pipe*

This section presents the qualitative results obtained from the CFD simulations. To thoroughly evaluate the flow physics within the sudden expansion pipe, the velocity contours, pressure contours, and streamline visualizations for all three turbulence models which are Standard k-ε, Realizable k-ε and k-ω SST are presented and compared.

#### *3.2.1 Velocity distribution analysis for three different turbulence models*

The velocity magnitude contours for the three models are shown in Figures 7(a) through 7(c). In all three cases, the flow enters with a uniform velocity and accelerates into a central high-velocity "jet," shown in red, as it passes the expansion step. However, the behaviour of this jet differs significantly between the models. As seen in Figure 7(a), the Standard k-ε model predicts a relatively quick decay of the high-velocity core, which dissipates a short distance downstream of the expansion, suggesting the model is predicting intense mixing with the surrounding fluid.

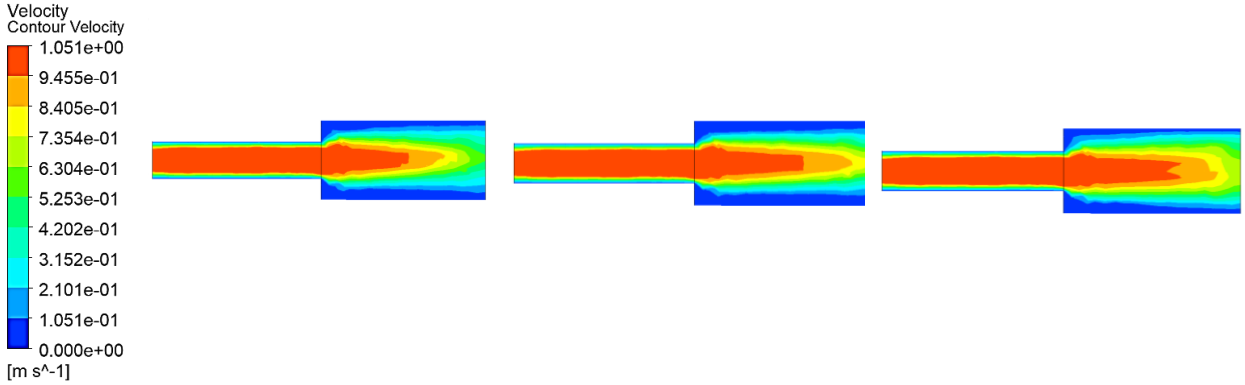


(a) (b) (c)

**Fig. 7.** Velocity magnitude contour (a) Standard k-ε (b) Realizable k-ε (c) k-ω SST models

In contrast, Figures 7(b) and 7(c) for the Realizable k-ε and k-ω SST models display a much longer potential core. In these models, the high-velocity jet extends significantly further towards the outlet before dissipating. This indicates that these formulations predict less diffusive mixing in the shear layer compared to the Standard k-ε model.

### *3.2.2 Static pressure distribution analysis for three different turbulence models*

The static pressure contours are presented in Figures 8(a) through 8(c). While all models capture the expected pressure drop at the expansion corner due to flow separation, the intensity varies. The Standard k-ε model in Figure 8(a) displays a large, intense region of low pressure which shown in dark blue, immediately following the step. The subsequent pressure recovers which is the transition from blue to green and yellow occurs rapidly, which is consistent with the rapid velocity decay observed in the previous section. Conversely, the Realizable k-ε and k-ω SST models in Figures 8(b) and 8(c) exhibit a noticeably different pattern. The low-pressure zone is less aggressive, and the pressure recovery occurs more gradually along the pipe length. The pressure contours for the Realizable k-ε and k-ω SST models are nearly identical, reinforcing the strong agreement between these two advanced formulations.

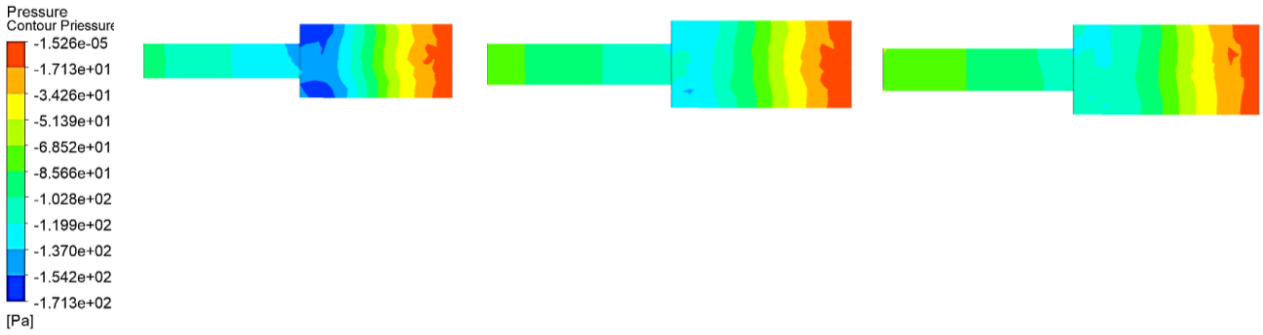


(a) (b) (c)

**Fig. 8.** Static pressure contour (a) Standard k-ε (b) Realizable k-ε (c) k-ω SST models

### *3.2.3 Streamline and recirculation zone analysis for three different turbulence models*

Streamlines coloured by velocity magnitude are utilized to visualize the flow separation and the recirculation zone, or the "bubble" of trapped fluid, in the corner of the pipe. In Figure 9(a), the Standard k-ε model shows a distinct recirculation zone; however, due to the model's known tendency to over-predict turbulent viscosity in separated flows, the reattachment point appears earlier, corresponding to the shorter central jet. Figures 9(b) and 9(c) for the Realizable k-ε and k-ω SST models reveal a more elongated flow structure. The streamlines clearly depict the shear layer separating the central jet from the recirculation zone, with flow reattachment occurring further downstream compared to the Standard k-ε case. The detailed swirling motion within the corner is captured effectively by both models, particularly the k-ω SST model, which is specifically designed to resolve near-wall behaviour more accurately.

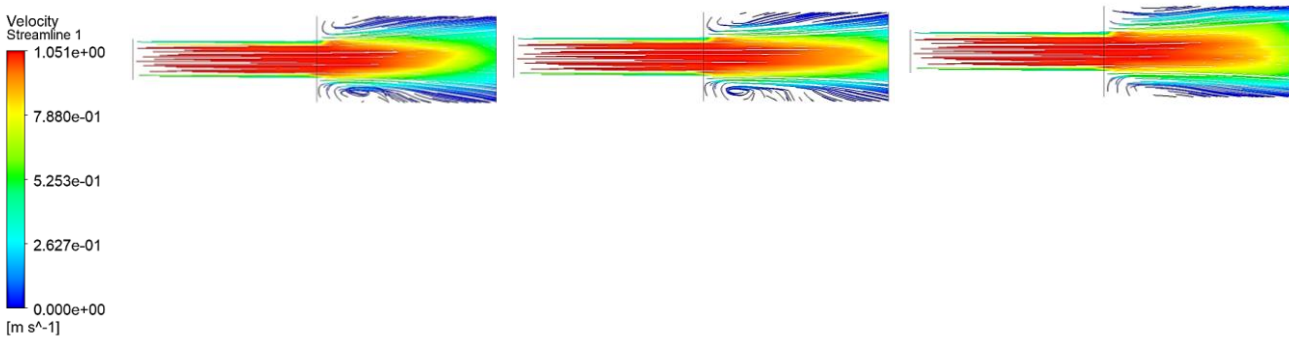


(a) (b) (c)

**Fig. 9.** Streamline visualization of the recirculation zone (a) Standard k-ε (b) Realizable k-ε (c) k-ω SST models

### *3.3 Quantitative Analysis of Flow Profiles for Three Different Turbulence Models*

Following the qualitative visual inspection, this section presents the quantitative comparison of the flow field. Data extracted along the pipe's centerline is plotted to precisely evaluate the differences in velocity decay and pressure recovery predicted by the three turbulence models.

#### *3.3.1 Quantitative comparison of centerline velocity profiles for three different turbulence models*

Figure 10 shows the velocity magnitude along the exact centerline of the pipe, as predicted by all three turbulence models. In the inlet section, all three models are in excellent agreement. However, a significant divergence occurs in the flow recovery zone. Consistent with the velocity contours observed in Figure 7(a), the Standard k-ε model predicts a rapid decay in centerline velocity. This confirms the model's prediction of intense turbulent mixing and a shorter potential core. In contrast, the Realizable k-ε and k-ω SST models show a much more gradual velocity decay. They predict that the high-velocity jet maintains its momentum further downstream, which quantitatively confirms the elongated jet structure observed in Figures 7(b) and 7(c).

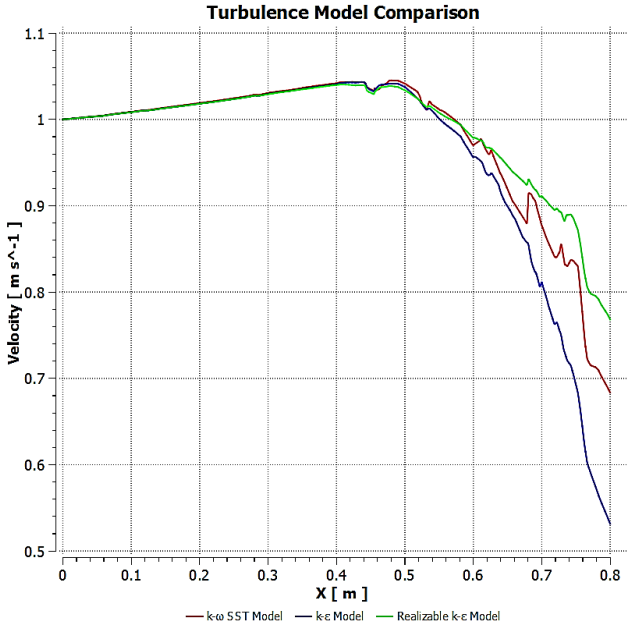


**Fig. 10.** Comparison of centerline velocity

### *3.3.2 Quantitative comparison of centerline static pressure distribution for three different turbulence models*

The static pressure distribution along the centerline is plotted in Figure 11. This graph highlights the most dramatic difference between the formulations. The Standard k-ε model model predicts a sharp and deep pressure drop immediately following the expansion. This aligns with the intense low-pressure zone seen in the contour plot which shown in Figure 8(a). Conversely, the Realizable k-ε and k-ω SST models both predict a significantly shallower pressure drop and a smoother recovery curve. The close agreement between these two curves suggests that the deep "dip" predicted by the Standard k-ε model is likely an over-prediction of the pressure loss caused by the recirculation zone.

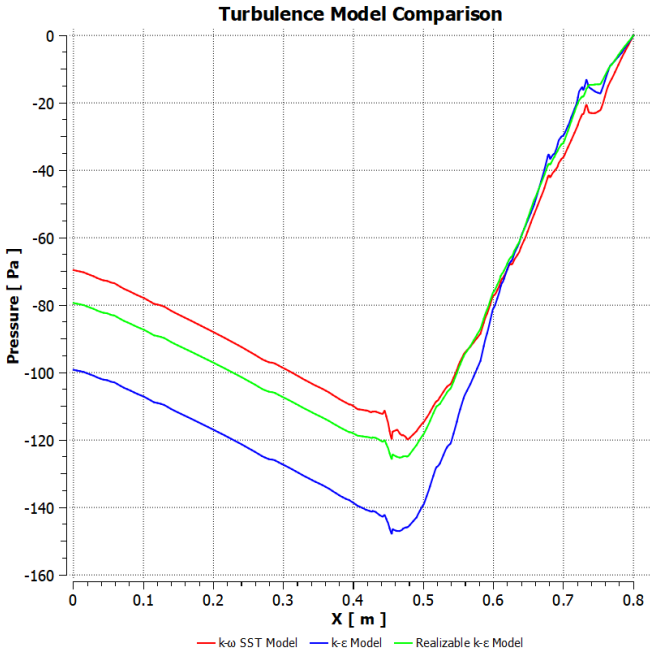


**Fig. 11.** Comparison of centerline pressure

### *3.4 Discussion of Model Performance and Accuracy*

The results presented in the previous sections highlight a significant finding: the choice of turbulence model has a profound impact on the simulation of flow through a sudden expansion. The standard $\mathrm{k}-\varepsilon$ model consistently emerges as a distinct outlier when compared to the realizable $k-\varepsilon$ and $k-\omega\ SST$ models.

The standard $\mathrm{k}-\varepsilon$ model's prediction of a much faster velocity decay and a significantly deeper, more aggressive pressure drop is not an arbitrary result. As discussed in the literature review, the standard $\mathrm{k}-\varepsilon$ model is known for its limitations in flows with strong flow separation and adverse pressure gradients. Its formulation tends to over-predict the generation of turbulent kinetic energy in regions of high shear, such as the layer between the central jet and the recirculation zone. This artificially high turbulence leads to excessive mixing, causing the model to predict a recirculation zone that is shorter and dissipates energy more aggressively, which is reflected in the sharp pressure and velocity drops.

In stark contrast, the realizable $k-\varepsilon$ and $k-\omega\ SST$ models show very close agreement with each other. This is also expected. Both models were specifically developed to address the failings of the standard model. The realizable $k-\varepsilon$ model uses a "realizable" formulation that prevents the over-production of turbulence in separated regions. The $k-\omega\ SST$ model, a hybrid approach, is

renowned for its superior performance in predicting flow separation and reattachment. Therefore, the close agreement between the realizable $k-\varepsilon$ and $k-\omega\ SST$ models provides high confidence that their shared prediction is a more physically accurate representation of the flow. The perceived accuracy of the standard $\mathrm{k}-\varepsilon$ model for this specific application is low, as it fails to capture the flow physics in the same way as the more advanced models. The results from the $k-\omega\ SST$ and realizable $k-\varepsilon$ models are considered far more reliable for this benchmark case.

## 4. Conclusions and Recommendations

### *4.1 Conclusions*

This project successfully simulated the turbulent flow through a 3D sudden expansion pipe, achieving the primary goals of investigating the complex flow dynamics and critically evaluating the performance of three RANS turbulence models. The study first established a validated grid, Mesh D, through a GIT, which was then used for the main comparative analysis.

The key finding of this study is that the choice of turbulence model has a profound impact on the simulation results. The Standard k-ε model consistently emerged as a distinct outlier. It predicted a significantly faster velocity decay in the recovery zone and a much deeper, more aggressive pressure drop compared to the other models. This discrepancy is directly linked to the model's known limitations in flows with strong separation, where it tends to over-predict turbulent mixing. In contrast, the Realizable k-ε and k-ω SST models showed very close agreement with each other, predicting a more stable central jet and a shallower, more similar pressure curve.

This close agreement between the Realizable k-ε and k-ω SST models provides high confidence that their shared prediction is a more physically accurate representation of the flow. Therefore, this study concludes that for this specific benchmark case, the perceived accuracy of the Standard k-ε model is low, and the realizable k-ε and k-ω SST models are far more reliable and accurate choices.

### *4.2 Recommendations for Future Work*

To build upon this study, two key recommendations are made. First, the numerical results, particularly key flow parameters like the velocity and pressure profiles predicted by the k-ω SST models, should be validated against published experimental data or established empirical correlations. This would provide a definitive measure of the simulation's true accuracy, moving beyond perceived accuracy. Second, a more advanced transient simulation could be performed to capture the unsteady, time-dependent behaviour of the turbulent eddies in the recirculation zone, which a steady-state RANS simulation cannot.

## References

[1] Lin, Mingzhao, and Yuyang Miao. "Importance and applications of fluid dynamics in civil engineering and mechanical engineering." *Highlights in Science, Engineering and Technology MECEME* 18 (2022): 247-252. https://doi.org/10.54097/hset.v18i.2681

[2] Gajbhiye, Bhavesh D., Harshawardhan A. Kulkarni, Shashank S. Tiwari, and Channamallikarjun S. Mathpati. "Teaching turbulent flow through pipe fittings using computational fluid dynamics approach." *Engineering Reports* 2, no. 1 (2020): e12093. https://doi.org/10.1002/eng2.12093

[3] Wong, M. K., L. Chang Sheng, CS Nor Azwadi, and G. A. Hashim. "Numerical study of turbulent flow in pipe with sudden expansion." *Journal of Advanced Research in Fluid Mechanics and Thermal Sciences* 6, no. 1 (2015): 34-48.

[4] Chew, John W., and Nicholas J. Hills. "Computational fluid dynamics for turbomachinery internal air systems." *Philosophical transactions of the royal society A: Mathematical, Physical and Engineering Sciences* 365, no. 1859 (2007): 2587-2611. https://doi.org/10.1098/rsta.2007.2022

[5] Ji, Guozhao, Meng Zhang, Yongming Lu, and Jingliang Dong. "The basic theory of CFD governing equations and the numerical solution methods for reactive flows." In *Computational Fluid Dynamics - Recent Advances, New Perspectives and Applications Recent Advances, New Perspectives and Applications* (2023): 1-30. https://doi.org/10.5772/intechopen.113253

[6] Idel'chik, I. E. "Handbook of Hydraulic Resistance, Coefficients of Local Resistance and of Friction, 1960." *English version, AEC-TR-6630* (1966).

[7] Lobanov, Pavel, Maksim Pakhomov, and Viktor Terekhov. "Experimental and numerical study of the flow and heat transfer in a bubbly turbulent flow in a pipe with sudden expansion." *Energies* 12, no. 14 (2019): 2735. https://doi.org/10.3390/en12142735

[8] Lahiouel, Yasmina, and Rachid Lahiouel. "Evaluation of energy losses in pipes." In *CFM 2015-22ème Congrès Français de Mécanique*. AFM, Maison de la Mécanique, 39/41 rue Louis Blanc-92400 Courbevoie, 2015.

[9] Uncu, Fatih, Benjamin François, Nicolas Buffaz, and Sébastien Le Guyader. "Assessment of RANS turbulence models on simplified geometries representative of turbine blade tip shroud flow." In *Turbo Expo: Power for Land, Sea, and Air*, vol. 86106, p. V10BT30A007. American Society of Mechanical Engineers, 2022. https://doi.org/10.1115/GT2022-80681

[10] Cant, Stewart. "SB pope, turbulent flows, Cambridge University Press, Cambridge, UK, 2000, 771 pp." *Combustion and Flame* 125, no. 4 (2001): 1361-1362. https://doi.org/10.1016/S0010-2180(01)00244-9

[11] Schiestel, Roland, and Bruno Chaouat. "Turbulence modeling and simulation advances in CFD during the past 50 years." *Comptes Rendus. Mécanique* 350, no. S1 (2022): 1-29. https://doi.org/10.5802/crmeca.114

[12] Launder, Brian Edward, and Dudley Brian Spalding. "The numerical computation of turbulent flows." In *Numerical Prediction of Flow, Heat Transfer, Turbulence and Combustion*, pp. 96-116. Pergamon, 1983. https://doi.org/10.1016/B978-0-08-030937-8.50016-7

[13] Versteeg, H. K., and W. Malalasekera. "Computational fluid dynamics: the finite volume method." *Harlow, England: Longman Scientific & Technical* (1995).

[14] Apalowo, Rilwan Kayode, and Cletus John Akisin. "CFD-based investigation of turbulent flow behavior in 90-deg pipe bends." *Journal of Applied Research in Technology & Engineering* 5, no. 2 (2024): 53-62.https://doi.org/10.4995/jarte.2024.20665

[15] Menter, Florian R. "Two-equation eddy-viscosity turbulence models for engineering applications." *AIAA Journal* 32, no. 8 (1994): 1598-1605. https://doi.org/10.2514/3.12149

[16] Menter, Florian R., Martin Kuntz, and Robin Langtry. "Ten years of industrial experience with the SST turbulence model." *Turbulence, Heat and Mass Transfer* 4, no. 1 (2003): 625-632.

[17] Lee, Minhyung, Gwanyong Park, Changyoung Park, and Changmin Kim. "Improvement of grid independence test for computational fluid dynamics model of building based on grid resolution." *Advances in Civil Engineering* 2020, no. 1 (2020): 8827936.https://doi.org/10.1155/2020/8827936

[18] Anderson Jr, John D. "Governing equations of fluid dynamics." In *Computational Fluid Dynamics: an Introduction*, pp. 15-51. Berlin, Heidelberg: Springer Berlin Heidelberg, 1992. https://doi.org/10.1007/978-3-662-11350-9

[19] Babu, Viswanath. *Fundamentals of Gas Dynamics 2nd Edition*. Springer, 2021.

[20] Blazek, Jiri. *Computational fluid dynamics: principles and applications*. Butterworth-Heinemann, 2015. https://doi.org/10.1016/B978-0-08-099995-1.00012-9